

PII: S0017-9310(97)00242-1

# Turbulent heat and fluid flow in a passage disturbed by detached perforated ribs of different heights

TONG-MIIN LIOU† and SHIH-HUI CHEN

Department of Power Mechanical Engineering, National Tsing Hua University, Hsinchu, Taiwan 30043, R.O.C.

(Received 8 August 1996 and in final form 29 July 1997)

**Abstract**—The spatially periodic turbulent heat transfer and friction in a rectangular passage of width-to-height ratio of 4:1 with perforated rectangular ribs detached from one wall have been studied using laser holographic interferometry, smoke-streak flow visualization, and pressure probing for rib-to-duct hydraulic diameter ratios ( $H/De$ ) of 0.081, 0.106, and 0.162 and Reynolds number ( $Re$ ) range of  $5 \times 10^3$ – $5 \times 10^4$ . The rib pitch-to-height ratio and the detached distance-to-rib-height ratio are 10 and 0.38, respectively. The laser-Doppler velocimetry measurements were performed to illustrate the local Nusselt number distribution. In contrast to the attached solid-type ribs which provide a monotonic decrease of thermal performance at a constant pumping power ( $\overline{Nu}_p/\overline{Nu}_s^*$ ) with increasing rib height, the detached perforated-type ribs give a best  $\overline{Nu}_p/\overline{Nu}_s^*$  at a moderate rib height  $H/De = 0.106$  for the lower  $Re$  range and a  $\overline{Nu}_p/\overline{Nu}_s^*$  independent of  $H/De$  for the higher  $Re$  range. In addition, the thermal performance of the detached solid-type ribs is found to be superior to that of the detached perforated-type ribs and the physical reason for the difference is addressed. © 1998 Elsevier Science Ltd. All rights reserved.

## INTRODUCTION

To remove local heat transfer deterioration around the rear concave corners of the attached solid ribs which have been extensively used for augmentation of heat transfer in many practical applications such as heat exchangers, gas turbine blades, and cooling panels used in a scramjet inlet [1–8], attached permeable ribs have been proposed and proved to be effective by researchers. Tanasawa *et al.* [9] measured the heat transfer coefficients for turbulent flows in a channel with perforated plate arrays mounted on two opposite walls in an in-line fashion by resistance heating method and thermocouple technique. Their results showed that surfaces with perforated plate arrays provided better thermal performance at a constant pumping power than those with slit plate arrays and fence arrays. Ichimiya and Mitsushiro [10] studied the heat transfer characteristics in a parallel plate duct with porous rib array mounted on one insulated wall which was opposite to the heated smooth wall. The mean heat transfer coefficient distribution measured by thermocouple technique was found to be two to four times that of the smooth duct, whereas friction factor measurements showed a decrease to two thirds to one fourth of that of the solid rib array. Recently, Hwang and Liou [11, 12] employed laser holographic interferometry (LHI) to investigate the effect of permeable rib arrays in in-line and staggered arrangements on the

periodically fully developed turbulent heat transfer in a rectangular channel. The effect of rib open-area-ratio ( $\beta$ ) was examined and a criterion of rib permeability was proposed. In addition, the permeable ribbed geometry provided a higher thermal performance than the solid-type ribbed one, and the best thermal performance occurred at  $\beta = 0.44$ .

In the papers quoted above, no data have been reported for turbulent heat transfer and friction in a duct with a detached square-rib array. Liou and Wang [13] and Liou *et al.* [14], therefore, performed such a study using LHI in developing and fully developed flow regions, respectively, for  $5 \times 10^3 \leq Re \leq 5 \times 10^4$  and  $0 \leq C/H \leq 1.5$ . The significant information reported by them is that there exists a critical clearance ratio,  $C/H = 0.38$ , above which the heat transfer augmentation is mainly achieved by the enhanced forced convection and turbulent transport along the heated wall, whereas below which the heat transfer augmentation is attributable to the extended surfaces provided by the square ribs and the approaching of the separated shear layer from the rib top rear corner toward the heated wall. However, the detached square ribs investigated by them were solid type. The present study thus intends to further examine the thermal performance of a permeable rib array positioned at a small distance from one wall.

Han [15] studied the effects of solid-rib height on the heat transfer and friction in a channel with two opposite rib-roughened walls (ribs attached to the walls and arranged in an in-line fashion) for rib-to-duct height ratios ( $H/De$ ) of 0.021, 0.04, 0.063 and rib

† Author to whom correspondence should be addressed.





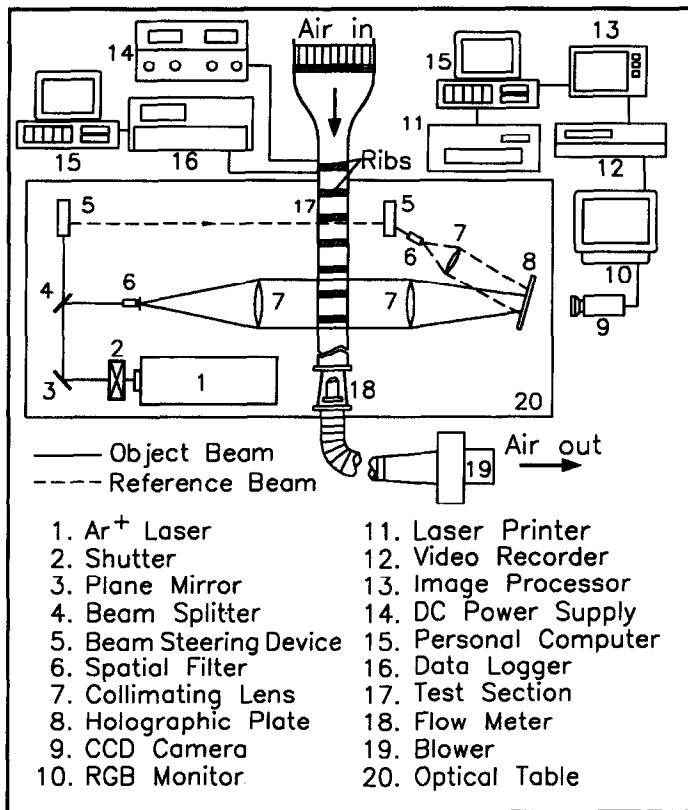


Fig. 2. Schematic drawing of overall experimental system.

previous results. The rib open-area-ratio and the clearance between the detached ribs and the bottom wall are fixed at  $\beta = 0.44$  and  $C/H = 0.38$ , respectively, since the previous studies indicated the maximum heat transfer and thermal performance enhancement attained by the permeable ribs and solid-type ribs at these  $\beta$  and  $C/H$  values [11, 14]. The parameters investigated include the rib height to duct hydraulic diameter ( $De = 64$  mm) ratio,  $H/De = 0.081, 0.106$ , and  $0.162$  (or rib-to-duct height ratio,  $H/2B = 0.13, 0.17$ , and  $0.26$ ), and the Reynolds number ( $Re$ ) (based on the hydraulic diameter and cross-sectional bulk mean velocity of the ribbed duct) from  $5 \times 10^3$ – $5 \times 10^4$ . Notice that the three rib heights examined are possibly used in small aircraft engines [8]. Since the present study is concerned with periodic fully developed heat and friction characteristics in ribbed ducts, the temperature and pressure drop data are taken in the range  $10 \leq X/De \leq 15$  and  $9.8 \leq X/De \leq 13.1$ , respectively. The spatially hydrodynamic and thermal periodicity in these regions has been verified in our previous work [13, 14], and thus is not elaborated on in the present work.

#### Two dimensionality

A check of two dimensionality of the temperature distributions across the test section width ( $Z$  direction) is necessary because the LHI is based on the

integral of the change in spanwise refractive index. Examples of wall temperature distribution in the  $Z$  direction at various Reynolds numbers have been presented in some previous works [3]. The scatter in spanwise direction is typically less than 5.7 percent of the duct spanwise average temperature. Another source of error is the presence of density gradients normal to light beam. By using the interferometry error analysis suggested in Goldstein [16], the resulting errors in the fringe (or temperature) shift due to the end effect associated with deviation from two-dimensionality and refraction effect associated with normal density gradient are 8 and 4.2%, respectively. Two dimensionality can also be checked in terms of spanwise distributions of the axial pressure different at various Reynolds numbers. Figure 3 shows that the maximum scatter in spanwise direction is typically within 4.2%.

#### Data processing

The Darcy friction factor of the periodically fully developed flow is expressed as:

$$f = [(-\Delta P/\Delta X) \cdot D_e]/(\rho \cdot U^2/2) \quad (2)$$

where  $\rho$  is the air density,  $U$  is the axial mean velocity, and  $\Delta P/\Delta X$  is evaluated by calculating the ratio of the pressure difference to the distance between two

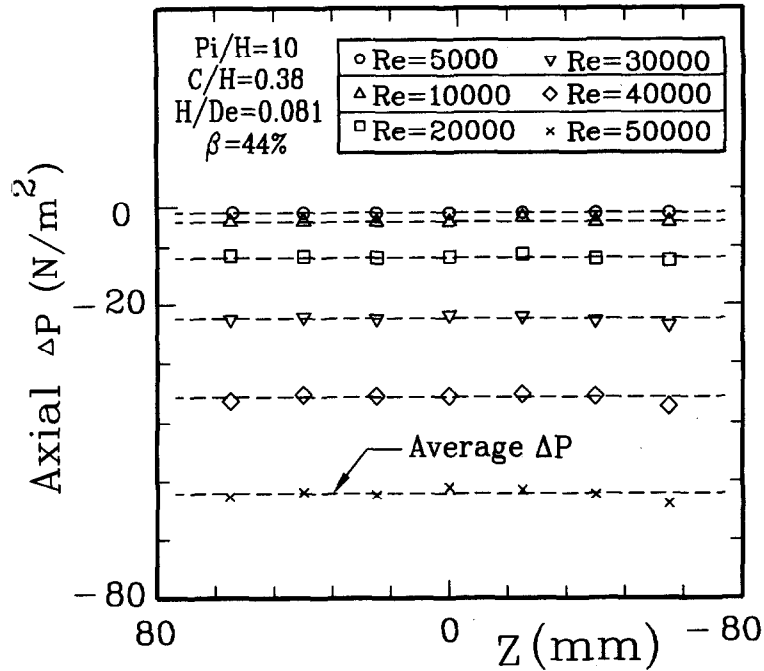


Fig. 3. Spanwise distribution of axial pressure drop at various Reynolds numbers.

successive Pitot tubes. A maximum 7.3% uncertainty of  $f$  is estimated.

The air temperature field  $T(X, Y)$  can be obtained from LHI interferograms through the following expression for a two-dimensional incompressible flow [17]

$$S_i - S_{i-1} = T_r \cdot \rho_r \cdot G_d \cdot 2A(1/T_{s_i} - 1/T_{s_{i-1}})/\lambda \quad (3)$$

where  $S_i - S_{i-1}$  is the fringe shift,  $S_i$  is the fringe order,  $G_d$  is the Gladstone–Dale constant, and  $\rho_r$  is the air density evaluated at reference temperature  $T_r$ .

The local Nusselt number  $Nu$  of the heated surface is defined by

$$Nu = -(dT/dY)_w \cdot D_e / (T_w - T_b) \quad (4)$$

where  $(dT/dY)_w$  is determined by curve fitting, based on a least-squares method through the near-wall values for temperature and fringe shift;  $T_w$  (local wall temperature) is obtained from the thermocouple output; and  $T_b$  (local bulk mean air temperature) is calculated from an energy balance,  $T_b = T_{in} + Q/(m \cdot C_p)$ , where  $m$  is air mass flow rate,  $T_{in}$  air temperature at duct inlet,  $C_p$  specific-heat at constant pressure, and  $Q$  the quantity of heat given to air from the entrance to the cross section under consideration of the duct and can be obtained by the integration of  $\int_0^z [k_r \cdot (dT/dY)_w \cdot 2A] \cdot dX$ . Note that both wall's normal temperature gradients are included in performing the integration. The maximum uncertainty of the local Nusselt number owing to  $T_b$  is estimated to be less than 8.1% for all of the cases by the uncertainty estimation method of Kline and McClintock [18].

The average Nusselt number for the spatially periodic region is evaluated by

$$\overline{Nu}_p = q_{conv} \cdot D_e / [k_r \cdot (\overline{T}_w - \overline{T}_b)] \quad (5)$$

where  $q_{conv}$  is the convective heat flux from the wall and is estimated by subtracting the heat loss from the supplied electrical input,  $\overline{T}_w$  is the average wall temperature along the lower ribbed wall in one rib pitch, and  $\overline{T}_b$  is the average bulk mean temperature of air. The maximum uncertainty of  $\overline{Nu}_p$  is estimated to be less than 9.8%. The average Nusselt number for fully developed turbulent flow in smooth circular tubes correlated by Dittus and Boelter [19],  $\overline{Nu}_s = 0.023 \cdot Re^{0.8} \cdot Pr^{0.4}$ , is used to normalize the local and average Nusselt number in the present study.

## RESULTS AND DISCUSSION

### Interference patterns

Figure 4 shows typical examples of the holographic interferograms around the perforated rib at two different Reynolds numbers. The mean flow direction is from left to right. The selected gap between the perforated rib and the bottom wall,  $C/H = 0.38$ , is working appropriately as a nozzle, as evidenced by the contraction and expansion of the interference fringes in front of, beneath, and behind the rib, resulting in increased number of thin fringes and narrow fringe spacings and, in turn, the steeper temperature gradients around the rib base and near the heated wall. A large amount of heat conducted from the heated wall thus is convected by the fluid which is

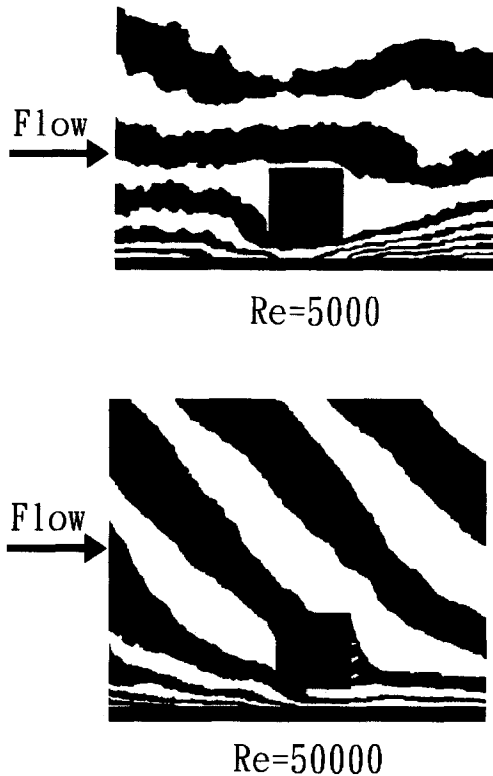


Fig. 4. Holographic interferograms at two different  $Re$  for  $C/H = 0.38$ ,  $Pi/H = 10$ ,  $H/De = 0.081$ , and  $\beta = 44\%$ .

accelerated through the gap between the rib base and the heated wall. There is a reduction of heat transfer rate on the rib top and rib rear face where the fringes are thick and the fringe spacings are relatively wide. As the Reynolds number increases from  $5 \times 10^3$  to  $5 \times 10^4$ , Fig. 4 further shows that the number of fringes between the rib and the bottom heated wall decreases due to the reduction in the difference between the  $T_w$  and  $T_b$  in the spatially periodic fully developed flow regimes with increasing  $Re$  [3]. Also note that the saw-shaped fringes behind the rib can only be observed for the case of  $Re = 5 \times 10^4$  since the perforated rib is permeable for  $Re \geq 2 \times 10^4$ .

#### Local heat transfer coefficient

From the interferograms the distributions of local Nusselt number ratio  $Nu/\overline{Nu}_s$  along the duct wall with detached perforated ribs in one pitch module can be calculated. Figure 5 depicts one example for  $H/De = 0.081$ ,  $\beta = 44\%$ ,  $C/H = 0.38$ ,  $Pi/H = 10$ , and  $Re$  from  $5 \times 10^3$  to  $5 \times 10^4$ . For the reason inferred from the variation of fringe patterns with  $Re$ , as addressed in the last section, and the fact that  $\overline{Nu}$  increases with increasing  $Re$  according to the Dittus–Boelter correlation [19] for a smooth duct flow, the level of  $Nu/\overline{Nu}_s$ , is expected to decrease with increasing  $Re$ . For a fixed  $Re$  Fig. 5 shows that higher values of  $Nu/\overline{Nu}_s$ , generally appear in the region around the rib ( $9 \leq X_N/H \leq 10$ , subscript  $N = \text{rib index}$ ), which can

be illustrated by the mean-velocity vector field of Fig. 6 obtained from the complementary Laser-Doppler velocimetry (LDV) measurements and is due to the core fluids' curving down and flowing around rib's bottom corner and to the flow acceleration through the gap. The LDV setup is the same as that described in Liou *et al.* [5] except for the replacement of the attached solid ribs by the present detached perforated ribs. For  $Re \geq 2 \times 10^4$ , there exists a local maximum  $Nu/\overline{Nu}_s$  near  $X_N/H = 0$  due to turbulence generated by the interaction of multi-jets emitting from rib's rear face since the rib is now permeable. For the  $Re$  range tested Fig. 5 depicts that  $Nu$  is larger than  $\overline{Nu}_s$  in the entire pitch module, a result different from that of duct flows with attached solid ribs which usually reveal  $Nu < \overline{Nu}_s$  in the region around the juncture ( $X_N/H = 0$ ) of rib's rear edge and duct wall due to nearly stagnant fluid flow around there.

Figure 7 shows a comparison of  $Nu/\overline{Nu}_s$  distributions between duct flows with detached ( $C/H = 0.38$ ) ribs of perforated-type ( $\beta = 44\%$ ) and solid-type ( $\beta = 0\%$ ) for  $H/De = 0.81$  and  $Re = 2 \times 10^4$ . As one can see, the local level of  $Nu/\overline{Nu}_s$  is lower for the case of detached perforated ribs (empty circle) than for the case of detached solid ribs (empty triangle), although both cases attain heat transfer augmentation ( $Nu/\overline{Nu}_s > 1$ ) in the entire pitch module. The reason for the above difference in  $Nu/\overline{Nu}_s$  level is that there exists vortex shedding, as revealed from Fig. 8, behind the detached solid-type ribs. The vortex shedding enhances heat transfer between the core fluids and near-wall fluids, and hence gives higher level of  $Nu/\overline{Nu}_s$ . Owing to the permeability, Fig. 4, of the detached perforated ribs, vortex shedding phenomenon is not observed for the case of  $\beta = 44\%$ . It should be mentioned here that the smoke flow visualization photograph presented in Fig. 8 was taken at  $Re = 2.3 \times 10^3$ . Using the feature of the flow at  $Re = 2.3 \times 10^3$  to explain the feature of Nusselt number at  $Re = 2 \times 10^4$  (Fig. 7) is not strictly sound. A further evidence of vortex shedding behind the detached solid-type ribs ( $C/H = 0.38$ ) at a Reynolds number close to  $Re = 2 \times 10^4$  would be valuable. To achieve this goal, an oil-film technique was carried out at  $Re = 2 \times 10^4$ ; however, the photo visibility was poor. A recent work performed by Bosch *et al.* [20] for the flow past a solid square cylinder placed near a wall provided the useful information. They performed dye-injection flow visualization in a water tunnel at  $Re = 2.2 \times 10^4$ . Their results showed the presence of periodic vortex shedding over the range of  $C/H = 0.35$  to 0.5. Below this range, the shedding motion was completely suppressed.

Another interesting comparison between the detached ( $C/H = 0.38$ ) and attached ( $C/H = 0$ ) perforated ribs ( $\beta = 44\%$ ) can be made from Fig. 7. Over most of the pitch range, except in the region two rib heights ahead of rib, the attached perforated ribs (solid circle) give higher  $Nu/\overline{Nu}_s$  level than the detached perforated ribs (empty circle). To explain

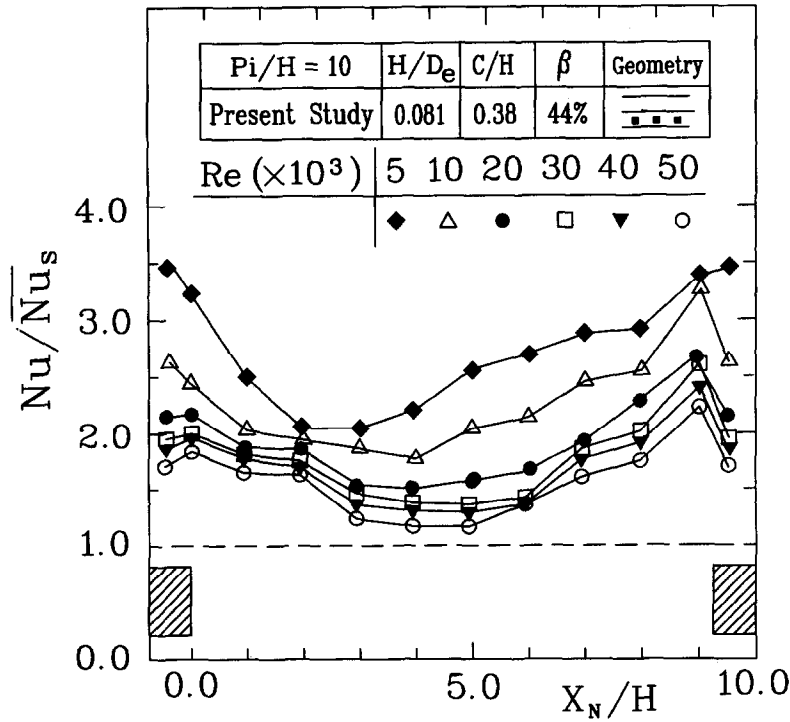


Fig. 5. Distributions of local Nusselt number ratio along the heated wall for various  $Re$ .

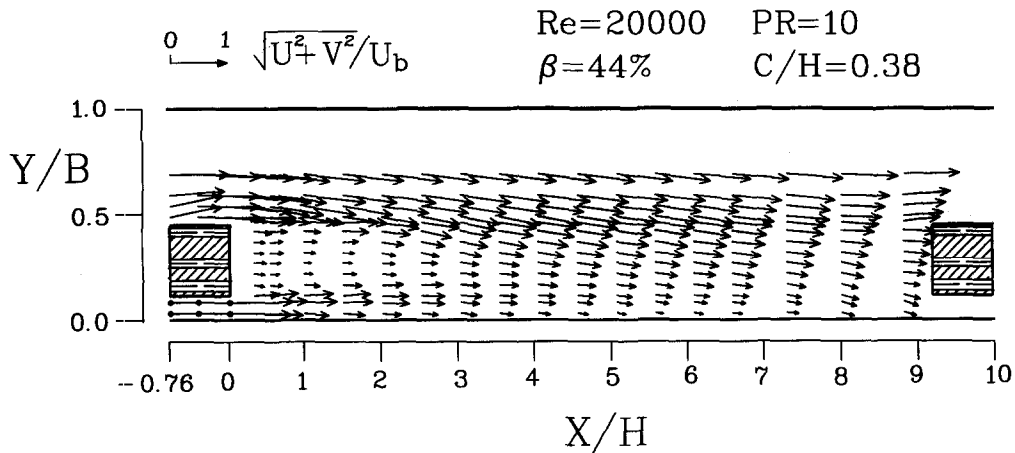


Fig. 6. Mean-velocity vector field for ribs of detached perforated-type.

the above result near-wall transverse mean velocity evolutions for the two cases compared are plotted in Fig. 9, where  $d$  is the distance from measured points to the duct wall. For  $7 < X/H < 9$  both Fig. 9 and Fig. 6 indicate the cold core fluids' curving down for the case of detached perforated ribs, thinning the boundary layer, enhancing forced convection, and thus resulting in a higher  $Nu/\overline{Nu_s}$  level than the case of attached perforated ribs which causes the fluids gradually moving upward in this region (Fig. 9). For  $2 < X/H < 7$  the attached perforated ribs give a higher  $Nu/\overline{Nu_s}$  level than the detached perforated ribs

since the effective flow reattachment occurs around  $X/H = 5$  for the case of attached perforated ribs. At short distances downstream of the perforated ribs,  $0 < X/H < 2$ , the attached perforated ribs can play the role of thermal-active ribs and conduct heat away from the hot duct wall in this region. In addition, the perforations further increase the heat transfer area of the thermal active perforated ribs. In contrast, the detached perforated ribs play as thermal-nonactive ribs whose perforations do not effectively increase the heat transfer area. As a result, the attached perforated ribs provide a higher  $Nu/\overline{Nu_s}$  level than the detached

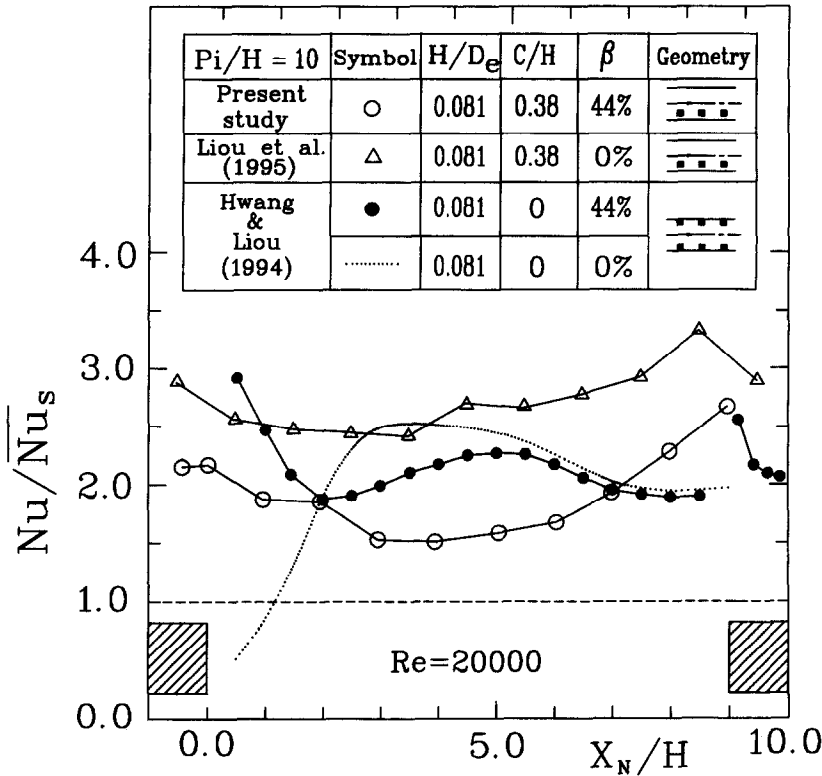


Fig. 7. A comparison of  $Nu/\overline{Nu_s}$  distributions among duct flows with ribs of detached perforated-type, detached solid-type, attached perforated-type and attached solid-type.

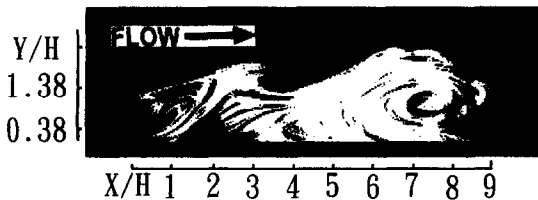


Fig. 8. Smoke-streak flow visualization photograph for  $H/De = 0.081$ ,  $\beta = 0\%$ ,  $C/H = 0.38$ , and  $Re = 2300$  (flow from left to right).

perforated ribs in the region of  $0 < X/H < 2$ . The effects of rib height on the heat transfer and friction for the case of detached perforated ribs will be presented in the following sections.

*Effects of rib height on heat transfer and friction*

Figure 10 depicts the distributions of  $Nu/\overline{Nu_s}$  in one pitch module for three rib heights and  $Re = 2 \times 10^4$ . In general, the local level of heat transfer augmentation for the duct flow with a detached perforated rectangular rib array increases with increasing rib height  $H/2B$ , although the increase is not linear. The average Nusselt number ratio for the detached perforated-type ribbed duct flows with three values of  $H/2B$  is plotted in Fig. 11 as a function of Reynolds number. Similar to the attached solid-type ribbed duct

flows [3, 15], Fig. 11 shows that the  $H/De$  dependence of  $Nu_p/\overline{Nu_{ps}}$  becomes weak as  $Re$  gets higher and  $Nu_p/\overline{Nu_s}$  decreases with increasing  $Re$  for the detached perforated-type ribbed duct flows due to the increase of  $\overline{Nu_s}$  with increasing  $Re$  being faster than that of  $Nu_p$ .

As far as the rib-height effect is concerned, Fig. 11 depicts that the  $H/De = 0.106$  case has a slightly higher  $Nu_p/\overline{Nu_s}$  for most of the  $Re$  range tested, a result different from that mentioned in the introduction for the attached solid-type ribbed duct flows which typically reveal an increase of average heat transfer coefficient with increasing  $H/De$  [3, 8, 15]. The rationale responsible for the main difference in the  $H/De$  dependence of  $Nu_p/\overline{Nu_s}$  between the above two types of ribs can be extracted from the discussion of local heat transfer coefficient presented earlier. For detached perforated ribs with  $C/H = 0.38$ , a large amount of heat conducted from the heated wall is convected by the accelerating fluids through the gap between the rib base and the heated wall and transported by the turbulence associated with the contraction and expansion of the flow around the gap region. Hence, there is a reduction of heat transfer rate on the rib top and rib rear face. These factors lead to the fact that for the detached perforated-type ribs the rib heat transfer surface area does not effectively increase with increasing  $H/De$ . In addition,

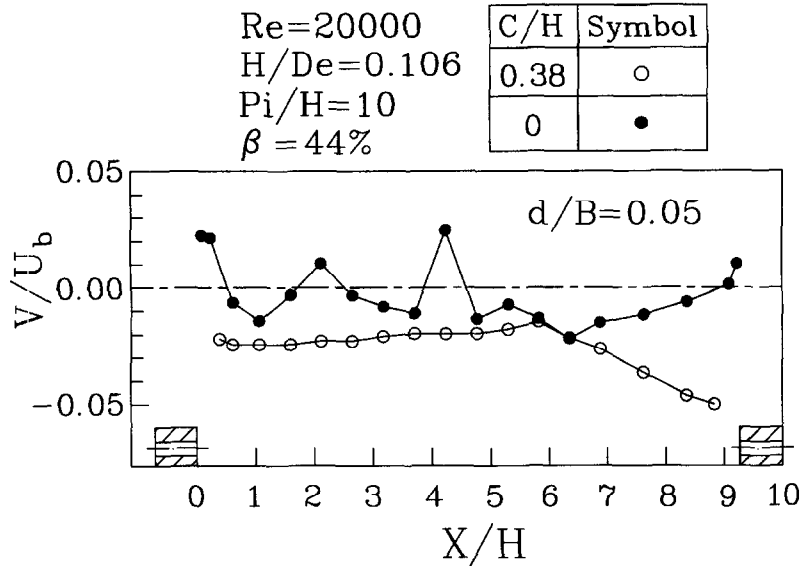


Fig. 9. Near-wall transverse mean velocity evolution for the attached and detached perforated ribs.

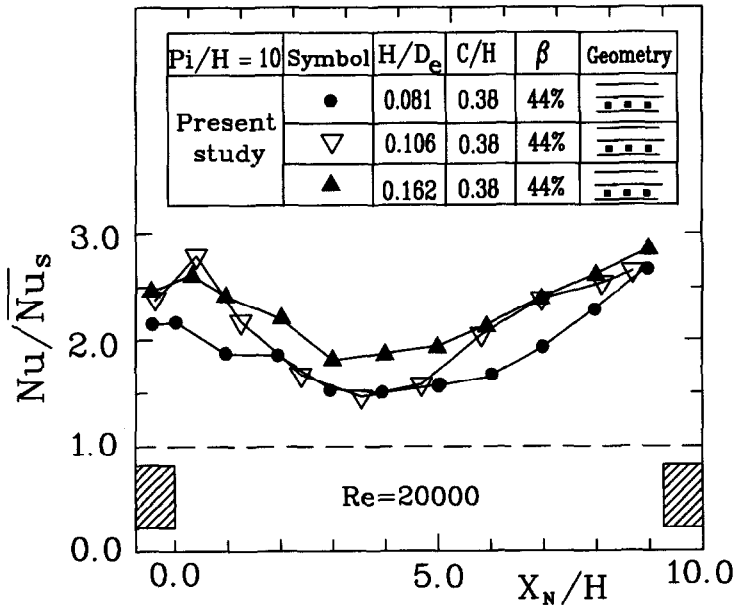


Fig. 10. Distributions of local Nusselt number ratio in one pitch module for three values of  $H/De$ .

although overall blockage increases to accelerate flow as  $H$  increases, the gap  $C$  also increases to offset that acceleration since  $C/H$  is fixed. Consequently, the average Nusselt number ratio in the present study does not monotonically increase with increasing  $H/De$ . With the values presented in Fig. 11 the dependence of the average Nusselt number on the dimensionless rib height and Reynolds number for the duct flows with detached perforated ( $\beta = 44\%$ ) ribs can be further correlated by an equation of the following form

$$\overline{Nu_p}/\overline{Nu_s} = 30.04 \cdot Re^{-0.20} \cdot (H/2B)^{0.31} \quad (5 \times 10^3 \leq Re \leq 5 \times 10^4) \quad (6)$$

where the constants are obtained by curve fitting, based on a least-squares method through the measured data. The average deviations of the experimental data from the above equation are  $\pm 3.5$ ,  $1.7$ , and  $3.1\%$  for  $H/De = 0.083$ ,  $0.106$ , and  $0.162$ , respectively.

Figure 11 also shows a comparison of  $Nu_p/\overline{Nu_s}$  between the duct flows with detached perforated-type

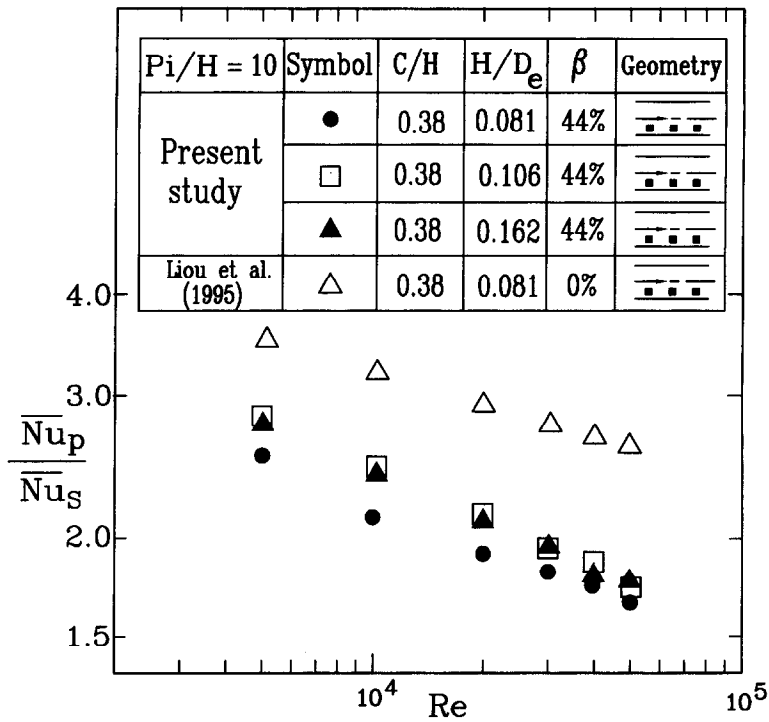


Fig. 11. Average Nusselt number ratio vs. Reynolds number for various  $H/D_e$ .

( $\beta = 44\%$ ) and solid-type ( $\beta = 0\%$ ) ribs for  $H/D_e = 0.081$ . The presence of vortex shedding for the latter, as addressed previously, results in a higher  $\overline{Nu_p}/\overline{Nu_s}$  than the former. Quantitatively, the levels of heat transfer augmentation of the detached perforated-type and solid-type ribbed ducts are approximately 1.7–2.5 and 2.5–3.5 times  $\overline{Nu_s}$ , respectively, for the test range of  $Re$  and  $H/D_e = 0.081$ .

The effects of  $H/2B$  on the Reynolds number dependence of the average friction factor for periodic fully developed duct flows with detached perforated-type ribs is shown in Fig. 12, where the result of detached solid-type ribs with  $H/D_e = 0.081$  is also included for comparison. As expected, all the curves show an increase of  $f$  with increasing rib height and a decrease of  $f$  with increasing  $\beta$  and  $Re$  for the range of parameters tested. For  $H/D_e = 0.081$ , the detached perforated-type and solid-type ribs increase the friction loss to approximately 1.3–2.6 and 3.5–4.9 times that of the smooth-wall case, respectively, for the range of parameters tested. A correlation for the effects of the dimensionless rib height and Reynolds number on the average friction factor of the present detached perforated-type ribs can be put in the following form:

$$f = 23.34 \cdot Re^{-0.46} \cdot (H/2B)^{0.47} \quad (5 \times 10^3 \leq Re \leq 5 \times 10^4) \quad (7)$$

The average deviations of the measured data from the correlation are  $\pm 12.6$ , 9.4, and 5.4% for  $H/D_e = 0.081$ , 0.106, and 0.162, respectively.

#### Thermal performance

Since the detached ribs disturb the core flow significantly, the detached-rib heat transfer augmentor also increases the friction loss. A thermal performance analysis at a constant pumping power is, therefore, worthwhile. In addition, the effect of rib height on the thermal performance of a duct flow with detached rectangular perforate-type ribs has not been studied in the past. Figure 13 shows such a study by comparing the average heat transfer coefficient for a duct with detached perforated-type of various heights with that for a smooth duct at a constant pumping power which is proportional to  $f^{1/3} \cdot Re$ . In Fig. 13  $\overline{Nu}_s^*$  is the average Nusselt number for a smooth duct with the flow rate at which the pumping power is the same as that required in the ribbed duct and its correlation has been described in detail by Liou and Hwang [3]. It is found from Fig. 13 that the improvement in  $\overline{Nu_p}$  of the duct flows with detached ( $C/H = 0.38$ ) perforated-type ribs is 1.3–1.9 times that of  $\overline{Nu}_s^*$  and the lower the pumping power parameter the higher the  $\overline{Nu_p}/\overline{Nu}_s^*$  is for the ranges of  $Re$  and  $H/D_e$  tested. For  $f^{1/3} \cdot Re < 3 \times 10^4$  the rib height to duct hydraulic diameter ratio of  $H/D_e = 0.106$  attains the best thermal performance at a constant pumping power among three values of  $H/D_e$  investigated; however, for  $f^{1/3} \cdot Re > 3 \times 10^4$  the  $\overline{Nu_p}/\overline{Nu}_s^*$  is nearly independent of  $H/D_e$  since the effects of  $H/D_e$  on the heat transfer rate and friction factor are approximately comparable at this range of Reynolds number. The above trend of the present work is unlike that of the attached solid-

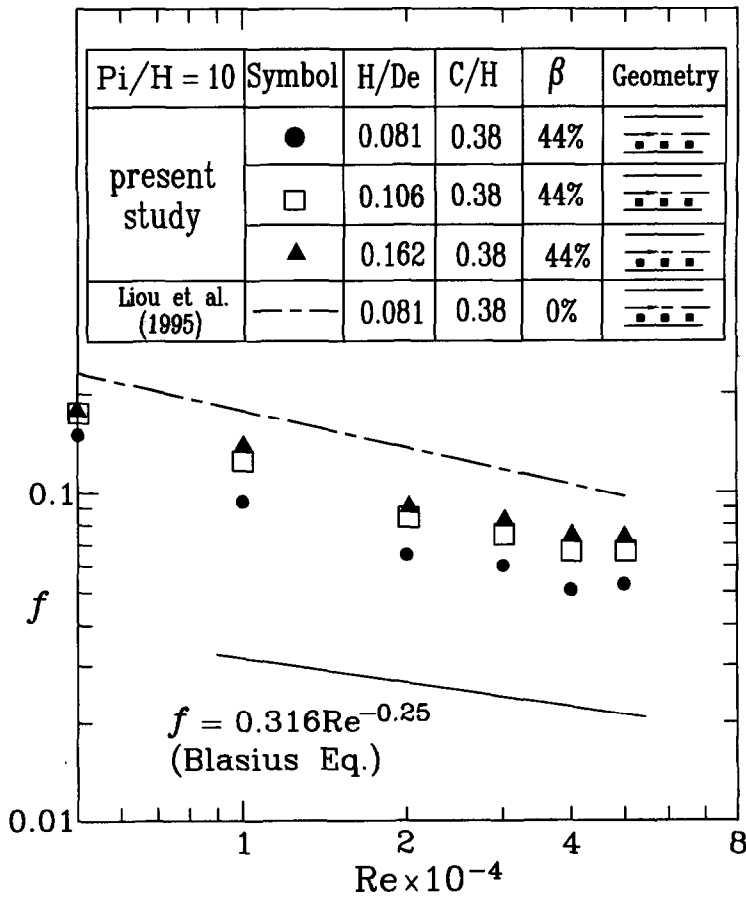


Fig. 12. Average friction factor vs. Reynolds number for various  $H/De$ .

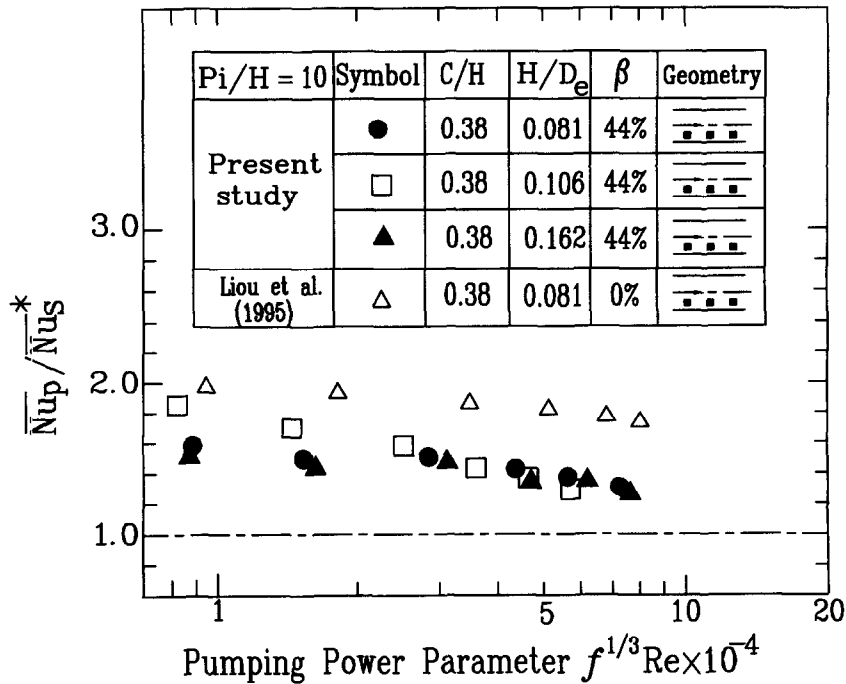


Fig. 13. Thermal performance comparison at a constant pumping power for various  $H/De$ .

rib case which usually shows a monotonic decrease of  $\overline{Nu_p}/\overline{Nu_s}^*$  with increasing  $H/De$  [8].

For a fixed  $H/De$  it is interesting to compare the thermal performances at a constant pumping power between duct flows with the present detached perforated-type ribs and previous detached solid-type ribs. Figure 13 provides such a comparison for  $H/De = 0.081$ . It is clear that  $\overline{Nu_p}/\overline{Nu_s}^*$  performance augmentation is less pronounced for a detached perforated-type ribbed duct,  $\overline{Nu_p} = 1.3\text{--}1.6 \overline{Nu_s}^*$ , than for a detached solid-type ribbed duct,  $\overline{Nu_p} = 1.8\text{--}2.0 \overline{Nu_s}^*$ .

### CONCLUSIONS

The effects of rib height ( $H/De$ ) on the spatially periodic turbulent heat transfer and friction in a rectangular passage with a rectangular perforated-type rib array detached from one wall have been studied with laser holographic interferometry and pressure measurements for the conditions tested in the present work. Compact correlations for the dependencies of the average Nusselt number and friction factor on the Reynolds number and  $H/De$  are obtained. For the ranges of Reynolds number and  $H/De$  examined the thermal performance ( $Nu_p$ ) attained by the present detached perforated-type ribbed duct is as high as 1.3–1.9 times that attained by a smooth duct ( $Nu_s^*$ ) at the same pumping power. Unlike the attached solid-type ribs, the detached perforated-type ribs do not give a monotonic decrease of  $\overline{Nu_p}/\overline{Nu_s}^*$  with increasing  $H/De$ . They provide a maximum  $\overline{Nu_p}/\overline{Nu_s}^*$  for the middle values of  $H/De = 0.106$  in the lower Reynolds number range tested and a  $\overline{Nu_p}/\overline{Nu_s}^*$  independent of  $H/De$  in the higher Reynolds number range tested.

For a fixed rib height it is found that the thermal performance of a detached perforated-type ribbed duct flow is less pronounced than that of a detached solid-type ribbed duct flow. As revealed from smoke-streak flow visualization, the reason is that the permeability of the former case break up the vortex roll-up and shedding phenomenon appearing in the latter case and useful for enhancing the heat transfer between the core fluids and near-wall fluids. Nevertheless, the interaction of multi-jets behind the detached permeable rib gives rise to a local maximum Nusselt number near the rib's rear face.

*Acknowledgement*—Support for this work was provided by the National Science Council of the Republic of China under contract No. NSC82-0401-E007-289.

### REFERENCES

- Han, J. C., Glicksman, L. R. and Rohsenow, W. M., An investigation of heat transfer and friction of rib-roughened surfaces. *International Journal of Heat and Mass Transfer*, 1978, **21**, 1143–1156.
- Bergles, A. E., Some perspectives on enhanced heat transfer—second generation heat transfer technology. *Transactions of the ASME, Journal of Heat Transfer*, 1988, **110**, 1082–1096.
- Liou, T. M. and Hwang, J. J., Turbulent heat transfer augmentation and friction in periodic fully developed channel flows. *Transactions of the ASME, Journal of Heat Transfer*, 1992, **114**, 56–64.
- Liou, T. M., Hwang, J. J. and Chen, S. H., Turbulent transport phenomena in a channel with periodic rib turbulators. *AIAA Journal of Thermophysics Heat Transfer*, 1992, **6**, 513–521.
- Liou, T. M., Wu, Y. Y. and Chang, Y., LDV measurements of periodic fully developed main and secondary flows in a channel with rib-disturbed walls. *Transactions of the ASME, Journal of Fluids Engineering*, 1993, **115**, 109–114.
- Acharya, S., Dutta, S., Myrum, T. A. and Baker, R. S., Periodically developed flow and heat transfer in a ribbed duct. *International Journal of Heat and Mass Transfer*, 1993, **36**, 2069–2082.
- Chang, B. H. and Mills, A. F., Turbulent flow in a channel with transverse rib heat transfer augmentation. *International Journal of Heat and Mass Transfer*, 1993, **36**, 1159–1169.
- Taslim, M. E. and Wadsworth, C. M., An experimental investigation of the rib surface-average heat transfer coefficient in a rib-roughened square passage. *40th ASME International Gas Turbine Aeroengine Congress Exposition*, 1994, 94-GT-162, Hague, Netherlands.
- Tanasawa, T., Nishio, S., Takano, K. and Tado, M., Enhancement of forced convection heat transfer in a rectangular channel using turbulence promoters. *Proceedings ASME-JSME Thermal Engineering Joint Conference*, 1983, Vol. 1. Hawaii, U.S.A., pp. 395–402.
- Ichimiya, K. and Mitsuhiro, Enhancement of the heat transfer of wide temperature range in a narrow flow passage (effects of porous-type turbulence promoters in normal temperature range). *Proceedings of Experimental Heat Transfer, Fluid Mechanics, and Thermodynamics*, ed. R. K. Shah, E. N. Ganic and K. T. Yang. Dubrovnik, Yugoslavia, 1988, pp. 659–664.
- Hwang, J. J. and Liou, T. M., Augmented heat transfer in a rectangular channel with permeable ribs mounted on the wall. *Transactions of the ASME, Journal of Heat Transfer*, 1994, **116**, 912–920.
- Hwang, J. J. and Liou, T. M., Heat transfer and friction in a rectangular channel with perforated ribs staggeringly mounted on two opposite walls. *Transactions of the ASME, Journal of Heat Transfer*, 1995, **117**, 843–850.
- Liou, T. M. and Wang, W. B., Laser holographic interferometry study of developing heat transfer in a duct with a detached rib array. *International Journal of Heat and Mass Transfer*, 1995, **38**, 91–100.
- Liou, T. M., Wang, W. B. and Chang, Y. J., Holographic interferometry study of spatially periodic heat transfer in a channel with ribs detached from one wall. *Transactions of the ASME, Journal of Heat Transfer*, 1995, **117**, 32–39.
- Han, J. C., Heat transfer and friction in channels with two opposite rib-roughened walls. *Transactions of the ASME, Journal of Heat Transfer*, 1984, **106**, 774–781.
- Goldstein, R. J., Optical measurement of temperature. In *Measurements in Heat Transfer*, 2nd edn, ed. E. R. G. Eckert and R. J. Goldstein. Hemisphere, Washington, D.C., 1976, pp. 241–294.
- Hauf, W. and Grigull, U., Optical methods in heat transfer. In *Advances in Heat Transfer*, Vol. 6, ed. J. P. Hartnett and T. F. Irvine, Jr. Academic Press, New York, 1970, pp. 133–136.
- Kline, S. J. and McClintock, F. A., Describing uncertainties on single-sample experiments, *Mech. Engrg.*, 1953, **57**, 3–8.
- Dittus, F. W. and Boelter, L. M. K., *Publications on Engineering*, Vol. 2. University of California at Berkeley, 1930, p. 443.
- Bosch, G., Kappler, M. and Rodi, W., Experiments on the flow past a square cylinder placed near a wall. *Experimental Thermal Fluid Sci.*, 1996, **13**, 292–305.